Journal of Power Sources 531 (2022) 231339

Contents lists available at ScienceDirect

Journal of Power Sources

journal homepage: www.elsevier.com/locate/jpowsour

Power and energy capacity tradeoffs in an all-aqueous copper thermally regenerative ammonia battery

Nicholas R. Cross [a], Matthew J. Rau [b], Serguei N. Lvov [c,d,e], Christopher A. Gorski [f], Bruce E. Logan [a,f], Derek M. Hall [c,d,*]

[a] Department of Chemical Engineering, Pennsylvania State University, University Park, PA, 16802, USA
[b] Department of Mechanical Engineering, Pennsylvania State University, University Park, PA, 16802, USA
[c] The EMS Energy Institute, Pennsylvania State University, University Park, PA, 16802, USA
[d] Department of Energy and Mineral Engineering, Pennsylvania State University, University Park, PA, 16802, USA
[e] Department of Materials Science and Engineering, Pennsylvania State University, University Park, PA, 16802, USA
[f] Department of Civil and Environmental Engineering, Pennsylvania State University, University Park, PA, 16802, USA

HIGHLIGHTS

- Theoretical maximum energy density of Cu_{aq}-TRAB was 9.5 Wh L^{-1}.
- Higher ammonia concentration increased power density but decreased energy density.
- Experimental energy density increased with copper concentration to 2.15 Wh L^{-1}.
- Highest thermal efficiency was 2.2% with 0.5 M Cu.

ARTICLE INFO

Keywords:
Thermally regenerative battery
Energy density
Flow battery
Energy efficiency

ABSTRACT

Thermally regenerative ammonia batteries (TRABs) can provide energy storage and produce electrical power from low-grade waste heat instead of electricity. The use of all-aqueous copper-based electrolytes has recently produced higher power densities than those achieved using previous TRAB approaches based on reversible metal deposition and dissolution processes, but further gains are possible in power and energy density. We investigated the limitations of power and energy density and how they are impacted by the electrolyte composition and discharge currents. By increasing the ammonia concentration from 1 to 5 M, the power density of the battery increased from 11.2 to 28.5 mW cm^{-2}, but the energy density decreased from 0.56 to 0.31 Wh L^{-1}. Increasing discharge current densities from 4 to 12.5 mA cm^{-2} increased the average power density during discharge from 2.4 to 5.9 mW cm^{-2} without appreciable losses in energy density. Increasing the copper concentration from 0.1 to 0.5 M increased both energy density to 2.15 Wh L^{-1} and energy efficiency to 2.2% but did not substantially impact the power density. These results represent the highest performance metrics achieved for a low-grade waste heat to electricity system.

1. Introduction

Low-grade waste heat (<130 °C) is a significant source of untapped energy in the US and around the world, with 60 TWh of energy dissipated into the environment each year by power plants and industry [1]. A variety of electrochemical and membrane-based systems are being researched to utilize this low-grade waste heat through implementation such as supplementing traditional thermal power systems or for household co-generation in a distributed power system. Among the technologies under investigation are thermo-electrochemical cells (TECs), thermally regenerative electrochemical cycles (TRECs), and thermally regenerative ammonia batteries (TRABs) [2]. Solid-state thermoelectric devices offer much simpler operation and system design than electrochemical systems, but exhibit lower power density and lack the ability to store energy [3]. Of the electrochemical and membrane-based systems, TECs and TRECs have higher thermal

* Corresponding author. The EMS Energy Institute, Pennsylvania State University, University Park, PA, 16802, USA.
E-mail address: dmh5373@psu.edu (D.M. Hall).

https://doi.org/10.1016/j.jpowsour.2022.231339
Received 1 December 2021; Received in revised form 15 March 2022; Accepted 16 March 2022
Available online 25 March 2022
0378-7753/

efficiencies but lower power densities, limiting their viability [2]. TRABs have the highest power densities of the electrochemical and membrane-based systems while having energy efficiencies that are competitive with the highest-performing low-grade heat technologies [4].

TRABs operate with similar operational conditions as other hybrid and conventional flow batteries. Battery electrolytes are contained in storage tanks which are pumped into an electrochemical reactor to produce or store electricity. Reactor size governs power capacity and tank size governs energy capacity. The majority of TRAB chemistries are currently hybrid flow battery concepts as they operate using deposition-based redox reactions that deposit and deplete metals at the electrodes [5]. Unlike most flow batteries, a unique aspect of TRABs is that they can use low-grade waste heat to recharge through an ammonia separation process. In TRABs, the addition of ammonia to the anolyte forms an electric potential difference between its two electrodes by complexing with electroactive species in the anolyte thereby reducing the equilibrium potential at the negative electrode. During thermal recharging, the depleted anolyte is converted to a new catholyte through the thermal separation of its ammonia which is then added to the depleted catholyte, fully charging the battery [6]. Most previous TRABs used inexpensive transition metals such as copper, nickel, and zinc, and have produced high peak power densities using specially designed membranes, alternative solvents, larger open circuit potentials, and custom porous electrodes [7–10]. However, these deposition-based chemistries have a range of issues such as poor coulombic efficiencies and low energy densities [5,9,11–18]. Nonetheless, some exceptions have been found. Through the use of silver as the active redox metal, it was shown that a TRAB could be cycled 100's of times and that power density and deposition uniformity could be improved through tailoring of the electrode microstructure [19,20]. Likewise, a new type of TRAB was recently developed that uses fully aqueous copper species where the redox reactions are mediated by porous carbon electrodes (Fig. 1) [21]. The all-aqueous copper TRAB (referred to as the Cu_{aq}-TRAB) used bromide and ammonia ligands to stabilize both the Cu(I) and Cu(II) complexes in solution. By stabilizing Cu(I) and having it as the desired redox state instead of Cu(0), the issue of poor anodic coulombic efficiency that was present in metal copper-based TRABs and resulted in their inability to be cycled due to irreversible loss of electrode material has been addressed.

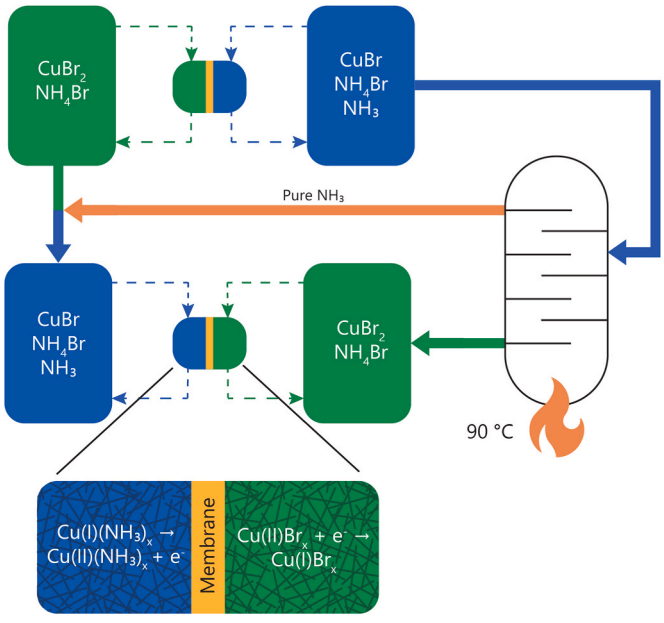

Fig. 1. Full system schematic of the electric discharge and thermal charging processes for the Cu_{aq}-TRAB.

The Cu_{aq}-TRAB showed high peak power density (35 mW cm^{-2}) and coulombic efficiency (98%), but the limits of the solution chemistry were not demonstrated and its performance in a flow cell was not well characterized. Many previous TRB investigations have explored the influence of electrolyte composition on power [5,9,11–13,15,22–28], but few have shown the impact on energy density, and none have demonstrated the tradeoffs between power and energy that results from the electrolyte composition. We investigated the impact of solution chemistry on the maximum copper concentration and therefore the theoretical energy density of the battery. Additionally, we characterized how the Cu_{aq}-TRAB performed in a flow cell with varying metal and ligand concentrations and discharge current densities to highlight strategies for maximizing both power and energy densities. The methods and metrics used in this study demonstrate that while peak and theoretical maximum values are valuable results, they do not properly represent the capability of the battery to operate in grid-scale applications.

2. Materials and methods

2.1. Reagents

Aqueous solutions were prepared with copper (II) bromide (99%, Acros Organics), copper (I) bromide (98%, Alfa Aesar), and ammonium bromide (99%, Alfa Aesar) salts. Ammonium hydroxide was added to the negative electrolyte from a 28 wt% ammonia Sigma-Aldrich stock solution. The electrolytes and cell assembly were purged with argon (99.997%, Praxair) prior to testing and dissolving of the copper (I) species to prevent oxygen contamination during testing. The reagents were prepared for each test such that the initial state of charge (SOC) was near 100%.

2.2. Solubility test assemblies and parameters

The maximum copper concentration based on solubility limits was estimated for a range of supporting electrolyte compositions through titrations. Solubility tests were performed using a multiport glass cell (#AKCELL2, Pine Instruments) (Fig. 2a). Solutions of just the background components of the electrolyte (ammonium salt and ammonia solution) at the desired concentration were created, then the copper salt (CuBr or $CuBr_2$) was added into the solution until the salt no longer dissolved. The temperature of the system was monitored and controlled to be at 25 ± 0.5 °C during all tests. The system was purged with argon during all Cu(I) tests to prevent the oxidation of the metal. After testing, the final volume of the solution was measured to adjust total solution volume to determine the molar concentration estimated to be the solubility limit of copper.

2.3. Full cell test assemblies and parameters

All full cell experiments were conducted using a zero-gap flow cell. The flow cell consisted of graphite plates with a column-pin flow field design (FuelCellStore) and a projected surface area of 25 cm^2, steel endplates, and fluorosilicone gaskets (Fig. 2b). All tests were performed using Nafion 117 as the membrane (FuelCellStore) and AvCarb G300A graphite felt electrodes (FuelCellStore), used as received. One hundred milliliters of each electrolyte were pumped from external reservoirs into the reactor stack with diaphragm pumps with perfluoroalkoxy (PFA) tubing and polytetrafluoroethylene (PTFE) fittings. The flow rate of the electrolytes had less than a 10% impact on peak power and limiting current density, thus it was concluded that flow rates were high enough that mass transfer effects on the polarization and discharge curves for this system were small enough to be neglected. The system was completely closed after the argon purge to prevent oxygen contamination during testing.

Flow cell measurements were performed with a Gamry Reference 3000. The test protocol was to conduct open circuit potential (OCP),

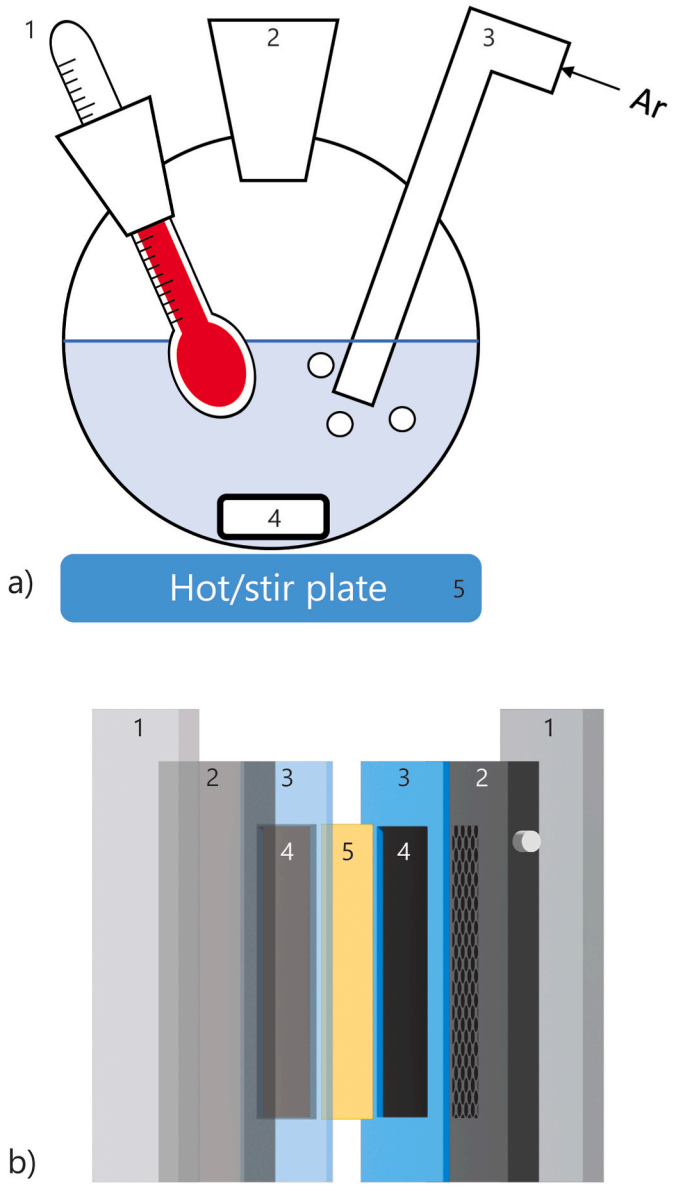

Fig. 2. a) Schematic of the experimental setup for solubility tests including (1) thermometer, (2) port for adding Cu salt, (3) tube for bubbling argon, (4) stir bar, and (5) heated stir plate. b) Schematic demonstrating the flow cell components including (1) steel end plates, (2) graphite flow fields, (3) fluorosilicone gaskets, (4) carbon felt electrodes, and (5) Nafion membrane.

linear sweep voltammetry (LSV), then electric charge/discharge cycling. The charge/discharge cycling always began with a brief charge cycle to return the electrolytes to 100% SOC to determine the maximum experimental energy density of the battery. LSV data was collected with a scan rate of 10 mV s^{-1} with the potential swept from 0 V *vs.* OCP to 0 V of cell potential. Charge/discharge tests were performed at a constant current of 4 mA cm^{-2}, unless otherwise specified, with upper and lower cutoff potentials of 1 and 0.35 V. Tests were ran at the ambient temperature in a fume hood (21 ± 1 °C).

2.4. Performance metric calculations

Theoretical energy storage density, u_{ideal} (Wh L^{-1}), was calculated using a simplified approximation that neglects state of charge and activity coefficients to compare the energy density of different solubilities, TRAB chemistries, and flow battery chemistries [29] as:

$$u_{ideal} = E^{0}_{cell} c_{tot} F \quad (1)$$

where E^{0}_{cell} (V) is the difference between the standard electrode potentials of interest (or standard cell voltage), and c_{tot} (mol L^{-1}) is the concentration of the electroactive species limiting the state of charge, and $F = 96485$ C mol^{-1}.

For full cell tests, the power density, p (mW cm^{-2}), was calculated as $p = jE_{cell}$, where j (mA cm^{-2}) is the current density and E_{cell} (V) is the cell potential. The power was normalized to 25 cm^2 since this is the projected geometric area of both the electrodes and the membrane. The experimental energy density, u_{exp} (Wh L^{-1}), was estimated by integrating the electric power, P (W), of the first discharge curve over time, t (s), and was normalized by the volume, V_{tot} (L), of the anolyte and the catholyte using:

$$u_{exp} = \frac{\int P\, dt}{V_{tot}}. \quad (2)$$

The solution volume was 0.2 L based on the combined liquid volume of catholyte and anolyte that was used for each test [30]. The electrochemical energy density was compared to the amount of heat input needed for the reboiler of the distillation column [4]. This value is referred to as the thermal energy efficiency and was estimated for the present study as:

$$\eta = \frac{\int P\, dt}{u_{charge}\, V_{ano}} \quad (3)$$

where u_{charge} (192 Wh L^{-1}) is the heat duty of the reboiler of the distillation column based on previous reports [7,22,31].

3. Results and discussion

3.1. Solubility limits and theoretical energy storage density

The maximum concentration of each copper oxidation state was highly dependent on the concentration of the bromide and ammonia in the solution. In the presence of only 5 M bromide, the Cu(I) species had a solubility of 2.5 M, while the Cu(II) species showed a lower solubility of 1.75 M (Fig. 3a), consistent with previous reports [32]. The maximum copper concentration for both Cu(I) and Cu(II) species was significantly lower when ammonia was present in solution. The maximum concentration of Cu(II) was 0.75 M for all ammonia concentrations tested except in the presence of 2.5 M bromide and 2 M NH_3 (0.4 M). In contrast, the maximum Cu(I) concentration increased from 0.1 M to 0.6 M as the ammonia in the solution increased from 1 M to 4 M. Thus, it was found that the limiting copper species for this TRAB was the $Cu(I)(NH_3)_x$ species, and its maximum concentration was 0.6 M based on a combination of 5 M NH_4Br and 4 M NH_3.

The equilibrium potentials of each electrolyte at the conditions that allow for the most copper to be fully-soluble (5 M NH_4Br and 4 M NH_3 in the anolyte) were estimated using the formation constants, as previously described [21]. The equilibrium potential was 0.557 V for the positive electrolyte, and −0.032 V for the negative electrolyte, resulting in the standard cell voltage of $E^{0}_{cell} = 0.589$ V. Using this value, a maximum copper concentration of 0.6 M, and Equation (1), a theoretical maximum energy density of 9.5 Wh L^{-1} was estimated for the Cu_{aq}-TRAB (Fig. 3b). The values used for calculation of the theoretical maximum energy storage density for each previous TRB chemistry were: Cu_m-TRENB – 0.1 M, $E^{0}_{cell} = 0.46$ V; Cu_m-TRAB – 0.3 M, $E^{0}_{cell} = 0.38$ V; Cu_{ACN}-TRB – 0.15 M, $E^{0}_{cell} = 1.2$ V. These concentrations represent the highest reported values from the literature, not necessarily the maximum possible, and the cell potentials were the difference in the standard redox potential of each reaction. However, it has been previously demonstrated that the equilibrium potentials of each reaction in the Cu_{aq}-TRAB depend on the concentration of the ligands in the electrolytes. This is

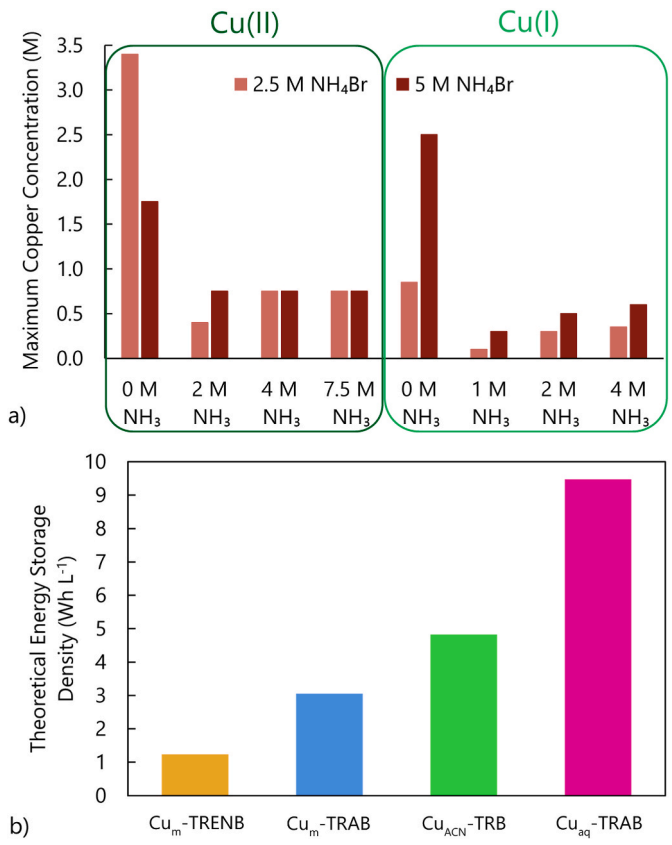

Fig. 3. a) Maximum soluble aqueous copper concentrations in various ammonium bromide concentrations and ammonia concentrations. b) Maximum theoretical energy storage density of different TRB chemistries based on their maximum redox species concentration and standard cell potentials [7,8,11].

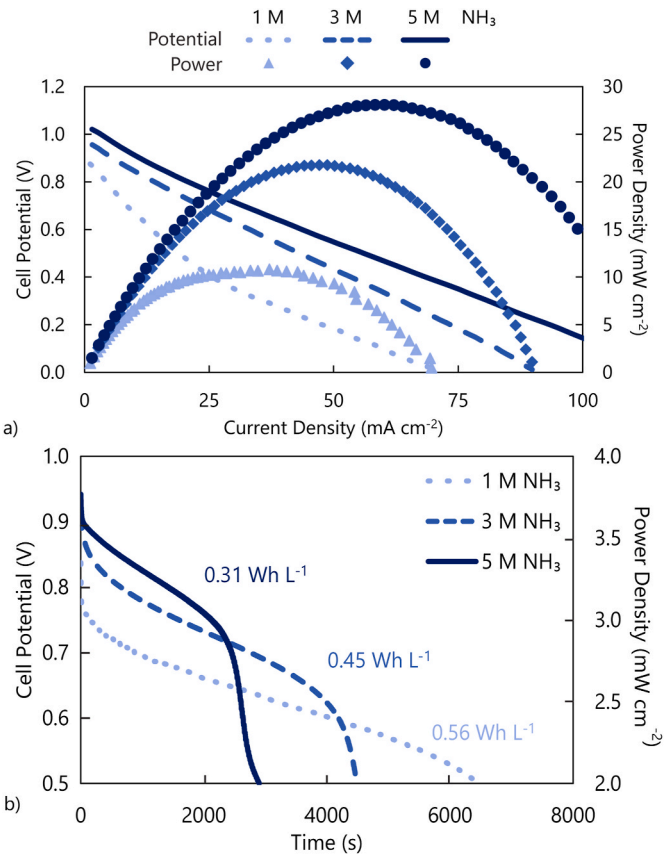

Fig. 4. a) Cell polarization and power density curves for varying NH_3 concentrations. b) Cell potential during constant discharge of the battery at 4 mA cm^{-2} at each concentration. Copper concentration was 0.1 M and NH_4Br concentration was 5 M in each electrolyte. Electrolytes were pumped at 200 ml min^{-1}.

likely to also be true of the previous TRB chemistries. Since there is no available literature on the impact of ligand concentration on the equilibrium potentials of these previous TRB chemistries, the maximum possible concentrations were not used since the cell potential would differ from the standard redox potential. The maximum energy density of the Cu_{aq}-TRAB is roughly twice that of previous TRBs based on their reported electrolyte conditions using the same method for estimating the theoretical energy storage density. This maximum energy density is lower than electrically charged flow batteries based on using vanadium chemical species of (>50 Wh L^{-1}) [30]. However, conventional flow batteries typically use more expensive materials and cannot be recharged using waste heat.

3.2. Impact of ammonia concentration on power and energy

Discharge and power density tests showed that the addition of ammonia increased power density but decreased energy density. For the Cu_{aq}-TRAB, the peak power density increased from 11.2 mW cm^{-2} to 28.5 mW cm^{-2} when increasing the NH_3 concentration from 1 M to 5 M (Fig. 4a). A contributing factor to this increase was the increase of the initial open circuit potential from 0.88 V to 1.03 V because the increasing free ligand concentration caused more complexation of the copper with ammonia.

Multiple previous investigations into deposition-based TRABs have demonstrated that increasing the NH_3 concentration results in higher peak power density [5,9,31], but the impact of NH_3 concentration on energy density was not usually shown. During discharge tests, the average power density of the battery increased with higher NH_3 concentration, with an average power density of 2.5 mW cm^{-2} with 1 M NH_3, and 3.1 mW cm^{-2} with 5 M NH_3 (Fig. 4b). Thus, while peak power density increased by 154%, the average power density during discharge only increased by 24%, demonstrating that peak power density is not a representative metric for evaluating performance during a full discharge cycle for the battery. However, the increasing NH_3 concentration reduced the energy density of the battery, as it decreased from 0.56 Wh L^{-1} at 1 M to 0.31 Wh L^{-1} at 5 M. While the cell potential of the 5 M NH_3 concentration discharge curve began higher than the 1 M NH_3 test, the total discharge time decreased from by 54%. Therefore, while increasing NH_3 concentration increased the peak power density by 154%, the energy density decreased by 44%. The decrease in energy density and total discharge time was likely a result of parasitic crossover of NH_3 from the anolyte to the catholyte. Increasing the free NH_3 concentration in the anolyte would increase its flux through the membrane. Evidence of a higher NH_3 flux was observed by a color change in the catholyte from brown to deep blue during discharge. Therefore, the tradeoff of power and energy density that can be controlled by electrolyte composition must be considered when designing a Cu_{aq}-TRAB for a specific application. If the application requires high power and short duration, having high NH_3 concentration is likely beneficial. Conversely, applications where energy storage is more critical than power output would benefit most from low NH_3 concentrations.

3.3. Impact of copper concentration on power and energy

Discharge and power density tests showed that increasing copper concentration produced a linear increase in energy density of the Cu_{aq}-TRAB, but it did not appreciably impact power density. The increase in copper concentration at a constant NH_3 concentration did not show produce any large changes in the polarization or power density curves

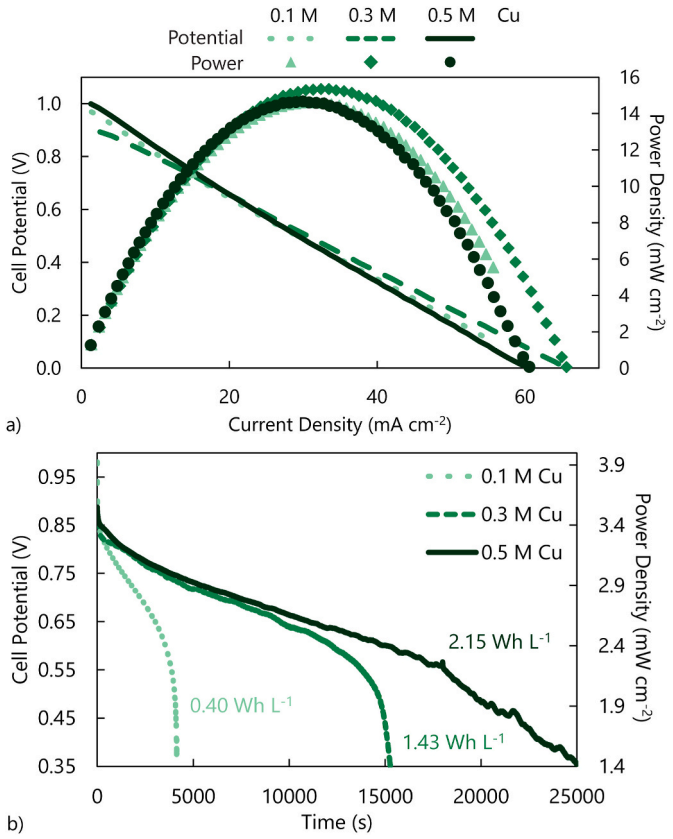

Fig. 5. a) Cell polarization and power density curves for varying copper concentrations. b) Cell potential during constant discharge of the battery at 4 mA cm^{-2} at each concentration. 5 M NH_4Br was used as the supporting electrolyte, and 4 M NH_3 was used in the anolyte. Electrolytes were pumped at 50 ml min^{-1}.

(Fig. 5a), with a peak power density of 14.6 ± 0.4 mW cm^{-2}. During discharge, the average power density was 2.8 mW cm^{-2} with 0.1 M Cu, and 2.5 mW cm^{-2} at 0.5 M Cu. The energy density increased linearly with copper concentration, as would be expected by Equation (2), with the energy density at 0.1 M being 0.40 Wh L^{-1} and at 0.5 M being 2.15 Wh L^{-1} (Fig. 5b). An added benefit of increasing the copper concentration was that more NH_3 was sequestered by complexation with the copper, resulting in less free NH_3 in the solution and slower parasitic crossover through the membrane. The thermal efficiency of the 0.5 M copper electrolyte was 2.2%, which is equal to the highest previously reported for a single-metal TRB at room temperature [4].

3.4. Influence of current density on discharge performance

Changing the discharge current impacted overall energy recovery. Increasing the applied current density during discharge increased the power density, but the impact on energy density was varied. Increasing the applied current density from 4 to 12.5 mA cm^{-2} doubled the average power density during discharge from 2.4 mW cm^{-2} to 5.9 mW cm^{-2} without a significant change in the energy density of 1.45 Wh L^{-1} (Fig. 6). The lack of significant change in energy density was unexpected because applying more current increases the overpotential of the reaction which could have decreased the energy produced by the battery. However, higher applied current also resulted in faster discharge of the battery, and as was shown in Section 3.2, self-discharge from NH_3 diffusion across the membrane is a major contributor to energy density losses at long discharge times. Therefore, the shorter discharge time from higher applied current resulted in less parasitic NH_3 diffusion and negated the impact of increasing overpotential that occurs with

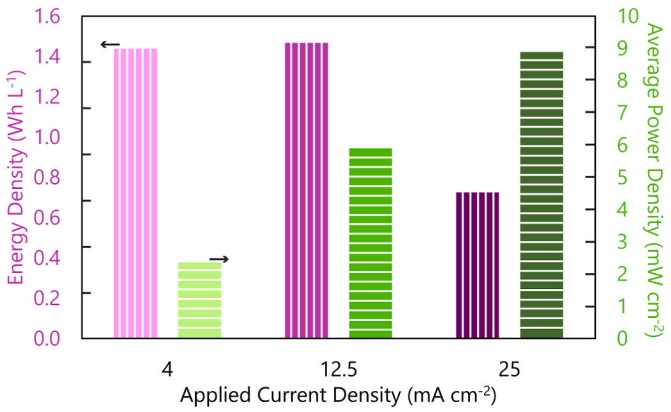

Fig. 6. Energy density and average power density during constant current discharge of the battery at varying applied current densities. 0.3 M copper was used in each electrolyte, 5 M NH_4Br was used as the supporting electrolyte, and 1 M NH_3 was used in the anolyte. Electrolytes were pumped at 200 ml min^{-1}.

increasing applied current. The shorter discharge time also resulted in smoother discharge curves due to less parasitic NH_3 diffusion, which produced more consistent power generation throughout the entire discharge cycle. When the applied current was increased to 25 mW cm^{-2}, the average power density increased to 8.9 mW cm^{-2}, but the increased overpotentials resulted in the energy density decreasing to 0.73 Wh L^{-1}.

3.5. Summary of TRAB performance

When comparing the Cu_{aq}-TRAB to previous TRB published chemistries at room temperature, it had improved performance across three major metrics for TRBs: power density, theoretical energy density, and thermal energy efficiency. These results clearly illustrate the need to report practical values such as average power during discharge and energy density/thermal energy efficiency in future TRB publications, as they are good indicators of the readiness level of the technology being studied to contribute electricity over a full cycle. The Cu_{aq}-TRAB was able to have the highest peak power density and the highest theoretical energy density (Fig. 7a), depending on solution chemistry and operation parameters. The highest peak power output was maintained during discharge, but high power resulted in a lower thermal energy efficiency (Fig. 7b). A maximum thermal energy efficiency for the Cu_{aq}-TRAB was 2.2%, which is the highest reported efficiency for all published TRBs with an average power output of 2.5 mW cm^{-2}. The thermal efficiency of the CuACN TRB was not reported, with only the theoretical efficiency reported of 2.2% [8]. The Cu_{aq}-TRAB had one of the highest efficiencies of these waste heat recovery technologies while still maintaining competitive power and energy densities. While vacuum distillation-concentrated redox flow batteries can have higher efficiency at about 4%, their power density is much lower (at 1 mW cm^{-2}) than the Cu_{aq}-TRAB, and their use of lithium is not as favorable as copper for economic and safety considerations [33].

4. Conclusions

The energy density and power density values demonstrated for the all-aqueous copper thermally regenerative ammonia battery were the largest reported for TRBs with some of the best power density and energy efficiency combinations identified for any low-grade waste heat to electricity system. With optimal solution conditions, the battery produced a peak power density of 28.5 mW cm^{-2} and energy density of 2.15 Wh L^{-1}. Results from the flow cell tests showed that the specific concentrations of NH_3 created tradeoffs between power and energy density. While increasing the NH_3 concentration from 1 to 5 M increased

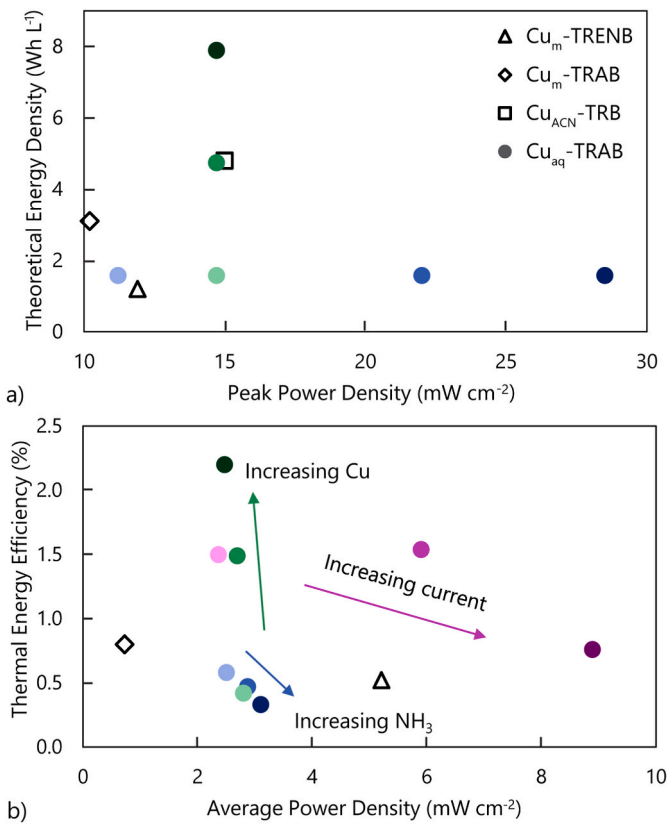

Fig. 7. Comparisons of a) peak power density and theoretical energy density and b) average power density during discharge and thermal energy efficiency between different Cu_{aq}-TRAB conditions and previous Cu-TRB chemistries at room temperature. The Cu_{aq}-TRAB data from the present study are presented as the filled circular symbols.

the peak power density from 11.2 to 28.5 mW cm^{-2}, the energy density decreased from 0.56 to 0.31 Wh L^{-1}. Increasing the copper concentration close to its maximum solubility, the experimental energy density of the battery was 2.15 Wh L^{-1}, and the thermal efficiency was 2.2%. Self-discharge of the battery through NH_3 crossover through the membrane was shown to be a primary contributor to energy density losses.

Support

This work was supported under DE-FOA-0002332.

Disclaimer

This report was prepared as an account of work sponsored by an agency of the United States Government. Neither the United States Government nor any agency thereof, nor any of their employees, makes and warranty, express or implied, or assumes any legal liability or responsibility for the accuracy, completeness, or usefulness of any information, apparatus, product, or process disclosed, or represents that its use would not infringe privately owned rights. Reference herein to any specific commercial product, process, or service by trade name, trademark, manufacturer, or otherwise does not necessarily constitute or imply its endorsement, recommendation, or favoring by the United States Government or any agency thereof. The views and opinions of authors expressed herein do not necessarily state or reflect those of the United States Government or any agency thereof.

CRediT authorship contribution statement

Nicholas R. Cross: Methodology, Investigation, Visualization, Validation, Writing – original draft. **Matthew J. Rau:** Conceptualization, Supervision, Methodology, Writing – review & editing. **Serguei N. Lvov:** Methodology, Supervision, Writing – review & editing. **Christopher A. Gorski:** Methodology, Writing – review & editing. **Bruce E. Logan:** Conceptualization, Methodology, Writing – review & editing. **Derek M. Hall:** Funding acquisition, Supervision, Conceptualization, Methodology, Writing – review & editing.

Declaration of competing interest

The authors declare that they have no known competing financial interests or personal relationships that could have appeared to influence the work reported in this paper.

References

[1] C. Haddad, C. Périlhon, A. Danlos, M.X. François, G. Descombes, Some efficient solutions to recover low and medium waste heat: competitiveness of the thermoacoustic technology, Energy Proc. 50 (2014) 1056–1069, https://doi.org/10.1016/j.egypro.2014.06.125.
[2] M. Rahimi, A.P. Straub, F. Zhang, X. Zhu, M. Elimelech, C.A. Gorski, B.E. Logan, Emerging electrochemical and membrane-based systems to convert low-grade heat to electricity, Energy Environ. Sci. 11 (2018) 276–285, https://doi.org/10.1039/c7ee03026f.
[3] S. LeBlanc, Thermoelectric generators: linking material properties and systems engineering for waste heat recovery applications, Sustain. Mater. Technol. 1 (2014) 26–35, https://doi.org/10.1016/j.susmat.2014.11.002.
[4] D. Brogioli, F. La Mantia, Innovative technologies for energy production from low temperature heat sources: critical literature review and thermodynamic analysis, Energy Environ. Sci. (2021) 1057–1082, https://doi.org/10.1039/d0ee02795b.
[5] F. Zhang, J. Liu, W. Yang, B.E. Logan, A thermally regenerative ammonia-based battery for efficient harvesting of low-grade thermal energy as electrical power, Energy Environ. Sci. 8 (2015) 343–349, https://doi.org/10.1039/c4ee02824d.
[6] F. Vicari, A. D'Angelo, Y. Kouko, A. Loffredi, A. Galia, O. Scialdone, On the regeneration of thermally regenerative ammonia batteries, J. Appl. Electrochem. 48 (2018) 1381–1388, https://doi.org/10.1007/s10800-018-1240-0.
[7] V.M. Palakkal, T. Nguyen, P. Nguyen, M. Chernova, J.E. Rubio, G. Venugopalan, M. Hatzell, X. Zhu, C.G. Arges, High power thermally regenerative ammonia-copper redox flow battery enabled by a zero gap cell design, low-resistant membranes, and electrode coatings, ACS Appl. Energy Mater. 3 (2020) 4787–4798, https://doi.org/10.1021/acsaem.0c00400.
[8] S. Maye, H.H. Girault, P. Peljo, Thermally regenerative copper nanoslurry flow batteries for heat-to-power conversion with low-grade thermal energy, Energy Environ. Sci. 13 (2020) 2191–2199, https://doi.org/10.1039/d0ee01590c.
[9] W. Wang, G. Shu, H. Tian, D. Huo, X. Zhu, A bimetallic thermally-regenerative ammonia-based flow battery for low-grade waste heat recovery, J. Power Sources 424 (2019) 184–192, https://doi.org/10.1016/j.jpowsour.2019.03.086.
[10] P. Chen, L. Zhang, Y. Shi, J. Li, Q. Fu, X. Zhu, Z. Lu, Q. Liao, Biomass waste-derived hierarchical porous composite electrodes for high-performance thermally regenerative ammonia-based batteries, J. Power Sources 517 (2022) 230719, https://doi.org/10.1016/j.jpowsour.2021.230719.
[11] M. Rahimi, A. D'Angelo, C.A. Gorski, O. Scialdone, B.E. Logan, Electrical power production from low-grade waste heat using a thermally regenerative ethylenediamine battery, J. Power Sources 351 (2017) 45–50, https://doi.org/10.1016/j.jpowsour.2017.03.074.
[12] L. Zhang, Y. Li, X. Zhu, J. Li, Q. Fu, Q. Liao, Z. Wei, Copper foam electrodes for increased power generation in thermally regenerative ammonia-based batteries for low-grade waste heat recovery, Ind. Eng. Chem. Res. 58 (2019) 7408–7415, https://doi.org/10.1021/acs.iecr.9b00616.
[13] W. Wang, G. Shu, H. Tian, X. Zhu, Removals of Cu(II), Ni(II), Co(II) and Ag(I) from wastewater and electricity generation by bimetallic thermally regenerative electrodeposition batteries, Separ. Purif. Technol. 235 (2020) 116230, https://doi.org/10.1016/j.seppur.2019.116230.
[14] W. Wang, H. Tian, G. Shu, D. Huo, F. Zhang, X. Zhu, A bimetallic thermally regenerative ammonia-based battery for high power density and efficiently harvesting low-grade thermal energy, J. Mater. Chem. A. 7 (2019) 5991–6000, https://doi.org/10.1039/c8ta10257k.
[15] Y. Shi, L. Zhang, J. Li, Q. Fu, X. Zhu, Q. Liao, Cu/Ni composite electrodes for increased anodic coulombic ef fi ciency and electrode operation time in a thermally regenerative ammonia- based battery for converting low-grade waste heat into electricity, Renew. Energy 159 (2020) 162–171, https://doi.org/10.1016/j.renene.2020.05.147.
[16] Y. Shi, L. Zhang, J. Li, Q. Fu, X. Zhu, Q. Liao, Y. Zhang, 3-D printed gradient porous composite electrodes improve anodic current distribution and performance in thermally regenerative flow battery for low-grade waste heat recovery, J. Power Sources 473 (2020) 228525, https://doi.org/10.1016/j.jpowsour.2020.228525.
[17] W. Wang, S. Yang, D. Huo, H. Tian, S. Li, X. Zhu, G. Shu, Understanding the reaction mechanism and self-discharge of a bimetallic thermally-regenerative ammonia battery, Electrochim. Acta 370 (2021) 137724, https://doi.org/10.1016/j.electacta.2021.137724.

[18] Y. Zhang, L. Zhang, J. Li, X. Zhu, Q. Fu, Q. Liao, Y. Shi, Performance of a thermally regenerative ammonia-based flow battery with 3D porous electrodes: effect of reactor and electrode design, Electrochim. Acta 331 (2020) 135442, https://doi.org/10.1016/j.electacta.2019.135442.
[19] M. Rahimi, T. Kim, C.A. Gorski, B.E. Logan, A thermally regenerative ammonia battery with carbon-silver electrodes for converting low-grade waste heat to electricity, J. Power Sources 373 (2018) 95–102, https://doi.org/10.1016/j.jpowsour.2017.10.089.
[20] N.R. Cross, D.M. Hall, S.N. Lvov, B.E. Logan, M.J. Rau, The impact of fiber arrangement and advective transport in porous electrodes for silver-based thermally regenerated batteries, Electrochim. Acta 388 (2021) 138527, https://doi.org/10.1016/j.electacta.2021.138527.
[21] R. Springer, N.R. Cross, S.N. Lvov, B.E. Logan, C.A. Gorski, D.M. Hall, An all-aqueous thermally regenerative ammonia battery chemistry using Cu(I, II) redox reactions, J. Electrochem. Soc. 168 (2021), 070523, https://doi.org/10.1149/1945-7111/ac1030.
[22] W. Wang, G. Shu, X. Zhu, H. Tian, Decoupled electrolytes towards enhanced energy and high temperature performance of thermally regenerative ammonia batteries, J. Mater. Chem. A. 8 (2020) 12351–12360, https://doi.org/10.1039/d0ta03236k.
[23] F. Vicari, A. Galia, O. Scialdone, Development of a membrane-less microfluidic thermally regenerative ammonia battery, Energy 225 (2021) 120221, https://doi.org/10.1016/j.energy.2021.120221.
[24] W. Wang, H. Tian, D. Huo, S. Yang, S. Li, X. Zhu, G. Shu, Modelling of a bimetallic thermally-regenerative ammonia flow battery for conversion efficiency and performance evaluation, J. Power Sources 499 (2021) 229943, https://doi.org/10.1016/j.jpowsour.2021.229943.
[25] W. Wang, G. Shu, H. Tian, X. Zhu, A numerical model for a thermally-regenerative ammonia-based flow battery using for low grade waste heat recovery, J. Power Sources 388 (2018) 32–44, https://doi.org/10.1016/j.jpowsour.2018.03.070.
[26] X. Zhu, M. Rahimi, C.A. Gorski, B. Logan, A thermally-regenerative ammonia-based flow battery for electrical energy recovery from waste heat, ChemSusChem 9 (2016) 873–879, https://doi.org/10.1002/cssc.201501513.
[27] M. Rahimi, A. D'Angelo, C.A. Gorski, O. Scialdone, B.E. Logan, Electrical power production from low-grade waste heat using a thermally regenerative ethylenediamine battery, J. Power Sources 351 (2017) 45–50, https://doi.org/10.1016/j.jpowsour.2017.03.074.
[28] M. Rahimi, Z. Schoener, X. Zhu, F. Zhang, C.A. Gorski, B.E. Logan, Removal of copper from water using a thermally regenerative electrodeposition battery, J. Hazard Mater. 322 (2017) 551–556, https://doi.org/10.1016/j.jhazmat.2016.10.022.
[29] D.M. Hall, J. Grenier, T.S. Duffy, S.N. Lvov, The energy storage density of redox flow battery chemistries: a thermodynamic analysis, J. Electrochem. Soc. 167 (2020) 110536, https://doi.org/10.1149/1945-7111/aba4e2.
[30] Y. Yao, J. Lei, Y. Shi, F. Ai, Y.C. Lu, Assessment methods and performance metrics for redox flow batteries, Nat. Energy 6 (2021) 582–588, https://doi.org/10.1038/s41560-020-00772-8.
[31] Y. Shi, L. Zhang, Y. Zhang, J. Li, Q. Fu, X. Zhu, Construction of a hierarchical porous surface composite electrode by dynamic hydrogen bubble template electrodeposition for ultrahigh-performance thermally regenerative ammonia-based batteries, Chem. Eng. J. 423 (2021) 130339, https://doi.org/10.1016/j.cej.2021.130339.
[32] J.M. Berger, R. Winand, Solubilities, densities and electrical conductivities of aqueous copper(I) and copper(II) chlorides in solutions containing other chlorides such as iron, zinc, sodium and hydrogen chlorides, Hydrometallurgy 12 (1984) 61–81, https://doi.org/10.1016/0304-386X(84)90048-3.
[33] I. Facchinetti, E. Cobani, D. Brogioli, F. La Mantia, R. Ruffo, Thermally regenerable redox flow battery, ChemSusChem 13 (2020) 5460–5467, https://doi.org/10.1002/cssc.202001799.